Available online at www.sciencedirect.com
ScienceDirect
International Journal of Multiphase Flow 34 (2008) 206–225
International Journal of Multiphase Flow
www.elsevier.com/locate/ijmulflow

Numerical simulation of the onset of slug initiation in laminar horizontal channel flow

P. Valluri, P.D.M. Spelt *, C.J. Lawrence, G.F. Hewitt

Department of Chemical Engineering, Imperial College London, South Kensington Campus, London SW7 2AZ, UK

Received 30 September 2006; received in revised form 28 June 2007

Abstract

Results are presented for the initiation of slug-type structures from stratified 2D, two-layer pressure-driven channel flow. Good agreement is obtained with an Orr–Sommerfeld-type stability analysis for the growth rate and wave speed of very small disturbances. The numerical results elucidate the non-linear evolution of the interface shape once small disturbances have grown substantially. It is shown that relatively short waves (which are the most unstable according to linear theory) saturate when the length of the periodic domain is equally short. In longer domains, coalescence of short waves of small-amplitude is shown to lead to large-amplitude long waves, which subsequently exhibit a tendency towards slug formation. The non-uniform distribution of the interfacial shear stress is shown to be a significant mechanism for wave growth in the non-linear regime.

Keywords: Slug flow; Two-phase flow; Stability

1. Introduction

The transition from stratified to slug flow is an important consideration in the design and operation of process equipment, especially in the transport of mixtures of gas with associated liquids (oil, condensate and/or water). Slug flow is associated with oscillations in pressure and flow rate and large surges of liquid, which can cause significant problems if the receiving facilities are not adequately sized. The pace of research is accelerating with the reliance on very long (hundreds of km) pipelines for multiphase transport from offshore fields in increasingly harsh and deepwater environments. Much research has naturally been conducted to determine the conditions under which the transition from stratified to slug flow occurs. The results are usually presented in the form of flow regime maps (e.g., Hewitt, 1982). The use of such flow maps is restricted by the fact that many parameters govern the transition. A dominant requirement for slugging is a minimum liquid level in the pipeline, which manifests itself in commonly used flow maps as a minimum superficial liquid velocity. Other

* Corresponding author. Tel.: +44 020 75941601; fax: +44 020 75945700.
E-mail address: p.spelt@imperial.ac.uk (P.D.M. Spelt).

0301-9322/$ - see front matter © 2007 Elsevier Ltd. All rights reserved.
doi:10.1016/j.ijmultiphaseflow.2007.09.001

important factors include the gas density, the liquid viscosity and the pipeline inclination (which change the liquid height required for transition, see Andritsos et al., 1989).

Several visual observations have provided some understanding of the physical mechanisms that lead to the onset of slugging (Andritsos et al., 1989; Fan et al., 1993). The first disturbances to appear on the interface are usually very small sinusoidal waves, which suddenly give rise to a large-amplitude wave that bridges the pipe and forms a slug. Sometimes a few large-amplitude waves coalesce with one another resulting in a longer wave before a slug is formed. Kordyban (1985), Davies (1992), Hale (2000) and Ujang et al. (2006), amongst others, presented images of the development of large-amplitude waves into slugs. The photographs show the development of small-amplitude waves on the crest of the large wave, just before the wave bridges the pipe.

Early theoretical work assumed a continuous growth of a small-amplitude long wave into a slug, driven by a Kelvin–Helmholtz instability (e.g., Taitel and Dukler, 1976). Wall shear and interfacial stress were accounted for by Lin and Hanratty (1986), but the long-wave assumption was retained, facilitating an integral momentum balance. Although the criteria for linear instability obtained in these early theoretical studies show quite good agreement with experimental conditions at the onset of slug formation, the underlying assumptions have been increasingly undermined by subsequent work and now seem unlikely to be justifiable. As early as 1989, Andritsos et al. reported observations invalidating the assumption that a single long wave develops continuously into a slug (made by Lin and Hanratty (1986)).

Much progress has been achieved in subsequent work, wherein the full Orr–Sommerfeld problem has been solved. Yiantsios and Higgins (1988) (amongst related work by others) presented extensive results from an Orr–Sommerfeld-type analysis for laminar pressure-driven two-layer channel flow, in the form of neutral stability curves. Results particularly relevant to the present work are presented in Section 2 below. A base-state velocity profile that corresponds to a turbulent flow has been accounted for in the analysis by Miesen and Boersma (1995) for sheared thin layers, and by Kuru et al. (1995) for conditions that are more representative of the onset of slug flow. It should be noted that these groups did not account for the modification of the turbulence structure by the waves, as considered by Belcher and Hunt (1993, 1998) for gravity waves. In any event, based on their results for the full linear stability problem, Kuru et al. (1995) criticised the long-wave assumption and the earlier inviscid analyses for slug initiation. Their results show poor agreement with results from the long-wave linear analysis and the inviscid theory, with the most unstable wavelength usually being of the order of the pipe diameter.

The previous results from Orr–Sommerfeld stability analyses of laminar two-layer channel flow, as well as for unbounded two-layer flows (e.g., Hooper and Boyd, 1983; Yecko et al., 2002; Boeck and Zaleski, 2005) show that the two relevant classes of instability mechanisms are an interfacial mode and shear modes (of Tollmien-Schlichting type) that occur at sufficiently large Reynolds numbers. Any of these modes can be dominant (with the TS modes evolving primarily in either of the two fluid layers), and may account for the instability of long (Yih, 1967) as well as short waves (Hinch, 1984; Boomkamp and Miesen, 1996), depending on flow conditions.

The mechanisms of linear instability in the case of slug initiation can be classified by using an energy balance based on the solution of the Orr–Sommerfeld problem. Boomkamp and Miesen (1996) performed energy balance calculations for the flow conditions of numerous previously conducted analyses and experiments. Although most cases considered are flows past a thin liquid layer, those authors reported that an important role is played by the interfacial mode caused by viscosity contrast in the waves studied by Andritsos and Hanratty (1987) and Kuru et al. (1995).

These findings are of course at odds with the earlier, inviscid stability analyses for slug initiation (e.g., Taitel and Dukler, 1976). In fact, Boomkamp and Miesen (1996) argued that the presence of viscosity, however small, eliminates any evidence of Kelvin–Helmholtz instability, i.e., that any observed instabilities would be governed by one of the alternative mechanisms mentioned above. The inviscid analysis of Morland and Saffman (1993) does recover a Kelvin–Helmholtz instability in the large-shear limit, but it only manifests itself at small wavelengths, where the inviscid analysis is no longer valid. The direct numerical simulations of the Navier–Stokes equations by Tauber et al. (2002) show that, under high shear, and upon using the inviscid solution as the initial condition for the flow field, the growth rates observed at short times are consistent with the inviscid analysis. But the relevance of Kelvin–Helmholtz analyses remains in dispute, even for mixing layers (Yecko et al., 2002). In Section 2 of the present work, after summarising the Orr–Sommerfeld analysis and

energy balance, we extend the range of the results of Boomkamp and Miesen (1996) to more representative cases of slug initiation, to clarify the mechanism for linear instability.

The subsequent weakly non-linear evolution has been investigated by Boomkamp (1998), who assumed that overtones are enslaved by the fundamental mode, so that Stuart–Landau theory could be used. He investigated a set of experimental conditions and showed that the bifurcation is supercritical. King and McCready (2000) included a spectrum of modes and accounted for all quadratic and cubic interactions for a particular set of flow conditions at which experiments had been conducted for gas–liquid flow. At sufficiently large values of the liquid Reynolds number, energy is transferred from the linearly dominant modes to the longest wave via the mean flow mode (i.e., the mode that does not vary in the flow direction), through quadratic interactions. These theoretical results showed encouraging agreement with experiments. The theory is, however, limited to modest mode amplitudes.

The main purpose of this paper is to use direct numerical simulations of the onset of slug initiation, in an effort to provide further insight into slug formation beyond the linear and weakly-non-linear regimes. Previous work in this area has focused primarily on two-phase mixing layers (e.g., Coward et al., 1997; Tauber et al., 2002; Boeck et al., 2006) and annular flows (e.g., Li and Renardy, 1999; Fukano and Inatomi, 2003). A common feature of the simulations of mixing layers is the evolution of waves into fingers that approach a point of pinch off and drop formation, rather than the formation of a wave of very large-amplitude, as in slug flows.

A further objective of the present work is to examine the interfacial stress distribution during the evolution of the waves. In the linear wave regime, several workers have related the wave growth to the phase difference between the wave and the perturbations of the normal and tangential interfacial stress (e.g., Belcher and Hunt, 1998; Benjamin, 1959; Miles, 1967; Davis, 1969; Thorsness et al., 1978). Many previous workers have attempted non-linear analyses using model wave equations, usually derived using some form of long-wave hypothesis. A critical feature of such work is the treatment of the interfacial stress. Very often the interfacial stress distribution is then related to the gas velocity by introducing an interfacial friction factor for which a closure relation is used (e.g., Taitel and Dukler, 1976; Andritsos and Hanratty, 1987). The fact is that very little is known about the true form of the stress distribution in the non-linear regime and how it changes during the wave growth. This is clearly of significant interest, since the waveform could have a strong effect on the stress distribution, providing a significant feedback mechanism for wave growth, as is evident from the linear analysis (e.g., Hanratty, 1983).

Some simplifications are made in order to facilitate accurate simulations. Firstly, the Reynolds numbers of the flows simulated are not large, and the resulting flow is laminar; also, the viscosity and density ratios are modest. Experimental evidence of slug initiation at values of the Reynolds number (based on the liquid flow) similar to or even lower than those in the simulations has been presented by Manolis (1995), for air–oil systems. The Reynolds number of the gas flow is much larger in experimental conditions than attempted here, but Manolis's data (as well as those by others, see, e.g., Mata et al., 2002) show no strong effect of the gas flow rate on the transition to slug flow. The main difference with larger gas flow rates is the absence of gas entrainment at the slug front (sometimes referred to as an elongated-bubble regime), the occurrence of which is indeed not the subject of the present paper. A second simplification made here is that the pipe geometry is assumed not to have a large effect on this process, so that only the two-dimensional problem is studied here. The main issue to be investigated is the transition from small-amplitude (and short-wavelength) waves to large-amplitude longer waves, stopping short of actual bridging events. Finally, this study is restricted to temporal instabilities; simulation of the evolution of convective instabilities would require excessive computational resources.

We use a level-set approach to track the deforming interface, with a projection-method Navier–Stokes solver [details of the present method can be found in Sussman et al. (1999) and in Spelt (2006)]. Some necessary modifications of the previous method are discussed in Section 3. An important and difficult issue is the convergence of numerical simulations of the evolution of waves that are initially of very small amplitude, so results from several convergence tests are presented. Results for the growth of small waves into large waves and their subsequent evolution, are presented and discussed in Section 4, and the paper is concluded in Section 5.

2. Governing equations and linear theory

We study here the evolution of a small-amplitude wave on the interface between fluids of different density and viscosity, as sketched in Fig. 1. The flow is driven by a pressure gradient along the length of channel

studied; the flow is horizontal, so that gravity is downwards. Periodic boundary conditions are used at the inlet and outlet. First, in this Section, we briefly summarise a linear stability analysis and present some key results. In this analysis, the growth rate and wave speed are determined for single harmonic modes. Of course this restriction could overpredict the value of critical parameters required for the onset of instability in practice. van Noorden et al. (1998) and South and Hooper (1999) have studied two-layer Poiseuille flow under conditions where single waves are linearly stable (following earlier work on the stability of e.g., single-fluid Couette flow). Their results show that, in cases that are stable according to a normal-mode analysis, the total energy can grow by a factor of 30 before the disturbance dies out. This is important, because it might be sufficient for non-linear effects to become significant. Similar analyses for two-fluid mixing layers have been carried out recently by Yecko and Zaleski (2005), who reported growth by factors of order 10^3. The present purpose is, however, to study the flow under conditions wherein waves are unstable. The results of the linear stability analysis will serve primarily as a benchmark test for the computations reported in subsequent sections. Also, the stream function perturbations of the most dangerous modes are used in an energy balance, to classify the physical mechanism that leads to instability in the flows considered in this paper.

2.1. Dimensionless parameters and linear analysis

The two fluids are denoted by $j = A, B$ with densities ρ_j, viscosities μ_j and interfacial tension γ, and flow through a channel of height H (see Fig. 1). The dimensional unperturbed depth of the lower fluid (B) is $\hat{h}$, and $\hat{\eta}$ is the dimensional perturbation of the interface position, so that the dimensional location of the interface is at $\hat{y} = \hat{h} + \hat{\eta}(\hat{x}, \hat{t})$. The subscripts $j = A, B$ are suppressed where they are not needed, and subscripts will also be used without ambiguity to denote partial differentiation. The length of the domain is considered to be equal to the wavelength of the imposed wave, λ. We introduce dimensionless variables, without caret, as follows:

$$\hat{\mathbf{x}} = H\mathbf{x}, \quad \hat{h} = Hh, \quad \hat{\eta} = H\eta, \quad \hat{\mathbf{u}} = V\mathbf{u}, \quad \hat{t} = (H/V)t, \quad \bar{p} = -\rho^A g(y-h) + (\rho^A V^2)\hat{p},$$

where $\mathbf{u}$ and p are the velocity and pressure, respectively. The velocity scale is chosen as $V = (\Phi/\rho^A)^{1/2}$, where Φ is the dimensional value of the imposed pressure gradient, such that in the base state discussed below, $p = -x$. The main dimensionless parameters are

$$Re = \frac{\rho_A VH}{\mu_A}, \quad m = \frac{\mu_B}{\mu_A}, \quad n = \frac{\rho_B}{\rho_A}, \quad Ca = \frac{\mu_A V}{\gamma}, \quad G = \frac{(\rho_B - \rho_A)gH^2}{\mu_A V}$$

and the dimensionless height of the lower fluid, h. In the base state, the interface is flat ($\eta = 0$), the flow is steady and unidirectional, $v = 0$, $u = U(y)$, and the pressure is linear, $p = -x$. The solution is then

$$U^A = -\frac{Re}{2}[y^2 - 1 - a(y-1)], \tag{1}$$

$$U^B = -\frac{Re}{2m}(y^2 - ay), \tag{2}$$

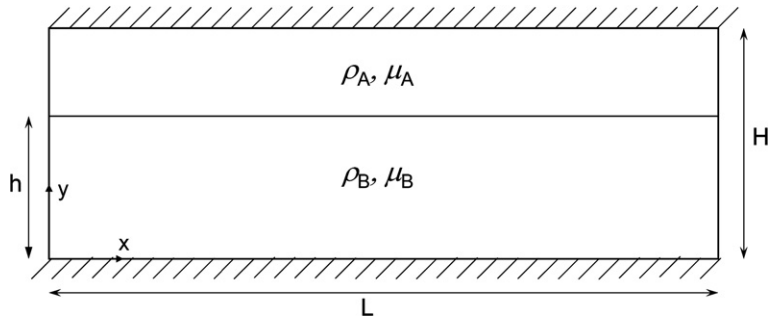

Fig. 1. Geometry and fluid properties.

where the coefficient a is chosen to give continuity of velocity at the interface:

$$a = \frac{h^2 + m(1-h^2)}{h + m(1-h)}.$$

We introduce a perturbation of the form:

$$\eta = \varepsilon\tilde{\eta}e^{i(kx-\omega t)}, \quad u = U(y) + \varepsilon\psi_y(y)e^{i(kx-\omega t)}, \quad v = -\varepsilon ik\psi(y)e^{i(kx-\omega t)}, \quad p = -x + \varepsilon\tilde{p}(y)e^{i(kx-\omega t)}.$$

Here ε is an arbitrary small parameter, $\tilde{\eta}$ the relative amplitude of the perturbation, ψ the (y-dependence of the) stream function of the perturbation, $\tilde{p}$ the corresponding (y-dependence of the) pressure, k the wavenumber ($=2\pi/\lambda$), taken to be real, and ω is the frequency, expected to be complex. If the perturbation is unstable, its temporal growth rate is given by $\mathrm{Im}(\omega)$.

Substitution of these expressions into the equation of motion, and dropping terms that are non-linear in the perturbed variables, results in an eigenvalue problem for the stream function $\psi(y)$, with eigenvalue $c = \omega/k$, similar to the Orr–Sommerfeld analysis for single-fluid flows. The eigenmodes $\psi(y)$ are determined numerically using a finite-difference approximation of the governing differential equation; this was found to be sufficient for the flows considered here. As similar analyses have been published before, the reader is referred to Yiantsios and Higgins (1988), Kuru et al. (1995) and South and Hooper (1999) for further details. Our results compare very well with those published by South and Hooper (1999). Their analysis is for the particular case of a two-layer flow with uniform density ($n = 1$, $G = 0$) and no surface tension.

The resulting eigenvalue spectrum is shown in Fig. 2 for a typical flow for which direct numerical simulations are presented in the following sections. We have rescaled the results to match those of South and Hooper (1999); in their notation, $U_{\max} = 0.14957$. It has been verified that these results converge when the finite-difference grid spacing is refined.

Typical results for the growth rate as a function of wave length are shown in Fig. 3a (the dimensionless parameters are as in Fig. 2). It is seen that the most dangerous mode corresponds to a rather short wave length of about $1.5H$, similar to the previous findings of Kuru et al. (1995) for turbulent flow. The growth rate is seen to be larger at smaller values of h in Fig. 3b. In the simulations presented in the following sections, h is set to the relatively large value of 0.7, in order to promote slug initiation rather then finger formation. Because of the computational effort required, the flows studied here are somewhat restricted. In most of the results, the remaining parameters are $Re = 500$, $G = 180$, $m = n = 10$ and $Ca = 10$. Further calculations showed no qualitatively different results, as discussed at the end of the paper. The flow conditions mentioned here correspond to Reynolds numbers based on the mean velocity for the upper and lower fluids as follows:

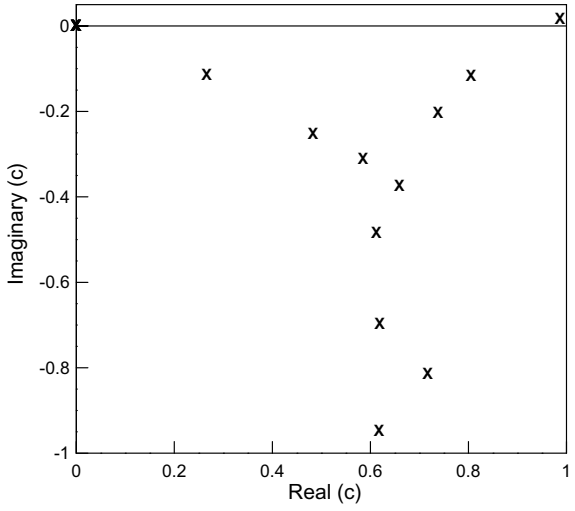

Fig. 2. Eigenvalue spectrum (in the complex plane) for the wave speed$c$: $h = 0.7$, $m = 10$, $n = 10$, $k = \pi/4$, $Re = 500$, $Ca = 10$ and $G = 180$.

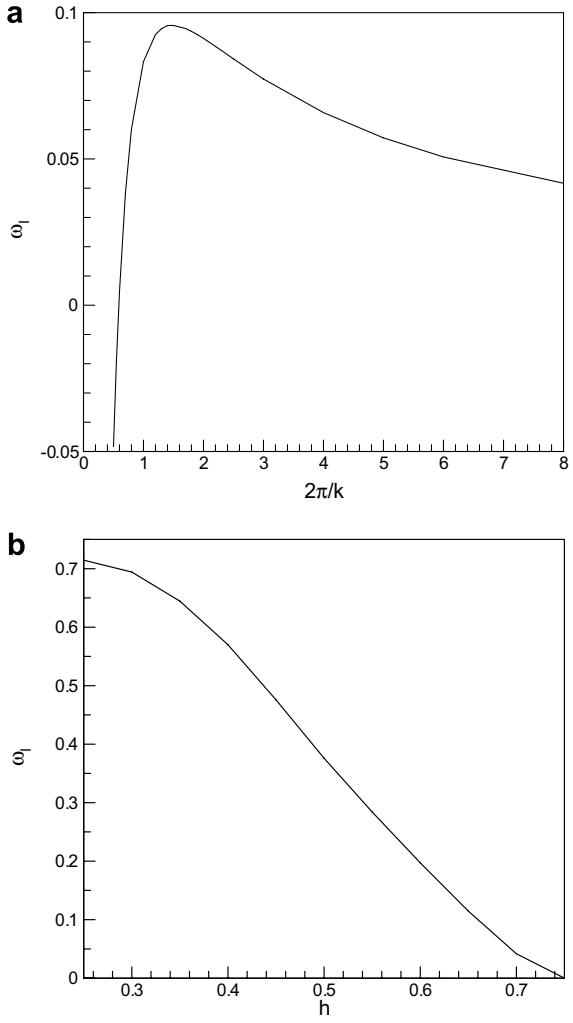

Fig. 3. Growth rate as a function of wave length (a) and interface height (b), from the linear analysis. Other values as in Fig. 2.

$Re_A^S = u_A^{\text{avg}}(H-h)\rho_A/\mu_A = 325$, and $Re_B^S = u_B^{\text{avg}} h\rho_B/\mu_B = 636$, where u_j^{avg} is the average base-state velocity for phase j. The linear analysis predicts a critical value of $Re_B^s = 99 \pm 4$ for $L = 8$.

2.2. Classification

We use the energy balance method of e.g., Hooper and Boyd (1983), Hu and Joseph (1989) and Boomkamp and Miesen (1996) to classify the linear instabilities studied here. This is necessary, because such a calculation has not been presented in previous work on the laminar problem (e.g., Yiantsios and Higgins, 1988). In this approach, the rate of change of the kinetic energy of the disturbance to the base state is obtained from the momentum equation. Upon integrating over a wave length ($\lambda = 2\pi/k$), the result is

$$\sum_{j=A}^{B} \text{KIN}_j = \sum_{j=A}^{B} \text{DIS}_j + \sum_{j=A}^{B} \text{REY}_j + \text{NOR} + \text{TAN}, \quad (j = A, B). \tag{3}$$

Here, DIS_j represents the viscous dissipation of the disturbed flow in each fluid, and is given in terms of the velocity components (u, v) by

Table 1
Energy distribution for $h = 0.7$, $m = n$=10, $Re = 500$, $G = 180$ and $Ca = 10$

λ	DIS_A	DIS_B	REY_A	REY_B	TAN	NOR
1.5	-2.2893×10^{-1}	-4.8638×10^{-2}	-1.3408×10^{-3}	5.8863×10^{-3}	3.2895×10^{-1}	-2.4576×10^{-5}
8	-1.3598×10^{-1}	-2.5090×10^{-2}	7.9891×10^{-4}	6.1465×10^{-3}	1.7612×10^{-1}	-1.0518×10^{-5}
9	-1.3232×10^{-1}	-2.4311×10^{-2}	8.9039×10^{-4}	5.9732×10^{-3}	1.7024×10^{-1}	-9.7226×10^{-6}

The wavelength, $L = 1.5$, corresponds approximately to the most dangerous mode.

$$\mathrm{DIS}_j = -\frac{m_j^2 h}{\lambda Re n_j} \int_{a_j}^{b_j} \mathrm{d}y \int_0^{\lambda} \left[2\left(\frac{\partial u_j}{\partial x}\right)^2 + \left(\frac{\partial u_j}{\partial y} + \frac{\partial v_j}{\partial x}\right)^2 + 2\left(\frac{\partial v_j}{\partial y}\right)^2 \right] \mathrm{d}x. \tag{4}$$

REY_j represents the energy contribution due to Reynolds stresses,

$$\mathrm{REY}_j = -\frac{n_j}{\lambda} \int_{a_j}^{b_j} \mathrm{d}y \int_0^{\lambda} \left[(-u_j v_j) \left(\frac{\mathrm{d}U_j}{\mathrm{d}y}\right) \right] \mathrm{d}x. \tag{5}$$

In Eqs. (3)–(5), $j = A$, $m_A = 1$, $n_A = 1$, $a_A = h$ and $b_A = 1$ for the upper fluid, and $j = B$, $m_B = m$, $n_B = n$, $a_B = 0$ and $b_B = h$ for the lower fluid. NOR and TAN represent the work done by the velocity and stress disturbances in the directions normal and tangential to the interface, respectively. NOR is given by,

$$\mathrm{NOR} = \frac{1}{\lambda} \int_0^{\lambda} [vS\eta_{xx}]_{y=h} \mathrm{d}x + \frac{1}{\lambda} \int_0^{\lambda} [vF\eta]_{y=h} \mathrm{d}x. \tag{6}$$

Here the first and second terms represent the work done against the deformation of the interface due to interfacial tension and gravity, respectively. S is an inverse Weber number given by $S = 1/(nhCaRe)$ and F is an inverse Froude number given by $F = Gh/(nRe)$. The tangential work done against interface deformation, TAN, is

$$\mathrm{TAN} = \frac{1}{\lambda} \int_0^{\lambda} [u_B \tau_B^{xy} - u_A \tau_A^{xy}]_{y=h} \mathrm{d}x, \tag{7}$$

where the component of the stress tensor is defined as

$$\tau_j^{xy} = \frac{m_j}{Re} \left(\frac{\partial u_j}{\partial y} + \frac{\partial v_j}{\partial x} \right). \tag{8}$$

In Table 1, the values of these terms in the energy balance are shown for several values of λ, including the most prominent mode ($\lambda = 1.5$). Evidently, the linear instability is driven by TAN. This finding is consistent with that of Boomkamp and Miesen (1996), who found that this term plays an important role in the energy balance for the slug initiation studies of Andritsos and Hanratty (1987) and Kuru et al. (1995).

The basic mechanism of initiation for such interfacial modes can generally be attributed to the viscosity or density contrast (Boomkamp and Miesen, 1996). A viscosity contrast leads to a discontinuity in the gradient of the base-state velocity profile at the undisturbed interface, which in turn causes a discontinuity in the disturbance velocity. This results in a source of kinetic energy of the disturbance. A density contrast gives rise to a similar source of disturbance energy, this time originating from a discontinuity in tangential stress across the undisturbed interface, at least for inclined channels. These initiating mechanisms are at the root of several mechanisms of instability in a variety of flow conditions (e.g., Kelly et al., 1989; Smith, 1990 for shear-driven falling films).

3. Method for direct numerical simulations

The main objective of this paper is to study the wave evolution beyond the linear regime, using full direct numerical simulations. The level-set method of Sussman et al. (1999) is used here, with the modifications presented in our previous work (Spelt, 2006) to eliminate global mass errors and to allow standard routines to be used in solving the resulting equations. One further modification is needed for the present simulations, namely

the implementation of periodic boundary conditions. Periodic boundary conditions rule out the standard multigrid routines that were used in our previous work to solve the Poisson equation for the pressure and the viscous predictor-type equation. Therefore, a block Gauss–Seidel technique that imposes the periodicity condition exactly is used here (Hirsch, 1988).

In the next section we present results from numerical simulations of the full equations of motion. The equations of motion were solved for a rectangular domain (see Fig. 1), subject to no-slip conditions at the top and bottom walls, and periodic conditions at the ends. The pressure drop was fixed during simulations (leading to a change in superficial velocity during wave growth that will be discussed in Section 4). The height and location of the wave crest were determined by linear interpolation. Early simulations were started from the base-state velocity field, with a small perturbation to the interface height. This resulted in significant oscillations in the observed growth rate. Therefore, the Orr–Sommerfeld solution for velocity and pressure fields was used as the initial condition in the simulations reported in the following section, unless indicated otherwise.

A concern specific to the nature of the flows simulated here is the representation of the discontinuity in physical properties across the interface. The standard procedure adopted in previous work (Sussman et al., 1999; Spelt, 2005) of smoothing these discontinuities over e.g., 1.5 times the grid spacing on either side of the interface will affect the dynamics of small waves. This has been recognised by several groups (Coward et al., 1997; Kang et al., 2000; Magnaudet et al., 2006). Coward et al. (1997) argued that the shear rate, rather than the viscosity, should be smoothed for simulations of flows in which shear along the interface dominates the stress tensor. In terms of a level-set formulation (the previous work cited above is for VOF methods), the smoothed value of the local viscosity, $\mu(\phi)$, is given by

$$\mu^{-1}(\phi) = \mu_A^{-1} + H(\phi)\mu_B^{-1}, \tag{9}$$

where ϕ is the local value of the level-set function (the distance to the interface; the sign of which identifies the fluid), and $H(\phi)$ is the smoothed Heaviside function. We have adopted this strategy in our simulations, and found that discretisation errors were reduced substantially, consistent with e.g., Coward et al. (1997). This strategy also yields a better agreement between our numerical and theoretical linear growth rates at early stages of wave growth (as would be shown later), similar to the findings of Boeck et al. (2006). It appears from the results presented e.g., in Figs. 11 and 12 below that also the later stages of wave growth considered here are dominated by shear.

A further complication is that simulating the approach to slug initiation starting from a wave of very small-amplitude requires many timesteps. It was found that, in some simulations, small discretisation errors around the interface can accumulate during the rather long period during which the wave amplitude is less than one grid spacing. Such disturbances may be attributed to the generation of spurious currents (e.g., Lafaurie et al., 1994; similar currents have been observed when using the present method, as mentioned by Spelt, 2005). These are understood to result from the discretisation of the surface-tension momentum-source term. Although the currents are usually small, the present simulations are over rather long integration times. The simulations are not extended to times at which the wave crest approaches the top wall of the channel, because the 3D geometrical effects for pipe flows would be very important at that stage.

Finally, the initial wave amplitude is taken to be much smaller than the grid spacing, unless indicated otherwise. The reason for this is that the theory is for infinitesimally small-amplitude. If the initial wave amplitude is not very small, the pressure disturbance is very large, rendering the linear analysis invalid. Therefore, we typically use an initial amplitude of $O(10^{-5})$. A convergence test for capillary waves is presented in the Appendix.

4. Results for flows with approach to slug initiation

We first investigate the evolution of the linear mode that was found to be the most unstable according to the linear theory presented in Section 2. Hence we consider the parameter values as in Fig. 2 but set $\lambda = 1.5$ (see Fig. 3). The length of the periodic cell L is set equal to the length of these waves. The growth rate and wave speed obtained from the simulations are compared with the Orr–Sommerfeld analysis in Table 2. The growth rate was determined from the height of the wave crest, averaging over the time interval wherein it grows approximately exponentially with time. It was verified that using the evolution of a Fourier transform of the wave shape gave virtually the same results (e.g., for the 192×128 grid in Table 2, the growth rate would

Table 2
Dependence of growth rate and wave speed on grid spacing

$N \times M$	ω_I	ω_R/k
64×96	0.066	2.912
128×192	0.088	2.908
256×384	0.096	2.908
Theoretical	0.096	2.906

Parameters used are $h = 0.7$, $m = 10$, $n = 10$, $k = 4\pi/3$, $Re = 500$, $Ca = 10$ and $G = 180$. The interface was perturbed with an initial amplitude of 2×10^{-5}.

be 0.087 instead of 0.088). The results from the simulations appear to converge to the analytical values. This is particularly encouraging, because it was seen in Section 3 that the instability is driven by the viscosity contrast, which has been smoothed in the simulations over a few grid points.

In Fig. 4 it is seen that the linear Orr–Sommerfeld solution remains a useful estimate for several decades of wave growth, when the initial amplitude is 0.02% of the channel height. It is not clear outright that the simulation method would be able to capture the wave evolution during stages where the amplitude is much smaller than the grid spacing. But the growth rate of the wave is seen in Fig. 4 not to change significantly when the wave amplitude becomes of the order of the grid spacing, which would suggest that the method can indeed be used for such small waves. Eventually, the wave saturates to a somewhat steepened structure, as can be seen in Fig. 5 (snapshots of the wave shape showed that the evolution only involved the growth and distortion of the initial wave). It could be anticipated that at larger values of Ca the wave may develop into fingers (e.g., Boeck et al., 2006), which is significant in the study of atomisation and droplet entrainment, but these relatively small-amplitude short waves appear at most to represent a very preliminary stage in the transition to slug flow.

In order to put these and subsequent results in context, we briefly investigate this non-linear evolution in more detail here, however. Fig. 6 shows the growth of the first four Fourier modes of the interface height for an initial amplitude of 10^{-3}. The evolution of the amplitude A_1 of the fundamental mode is compared in the figure with the solution of the Stuart–Landau equation,

$$\frac{dA_1}{dt} = \omega_I A_1 - \beta A_1^3, \tag{10}$$

using a fitted value for the Landau constant β. Given that the linear growth rate is somewhat underpredicted by the full numerical simulations at the grid spacing used (cf. Table 2), we have also used a fitted value in the

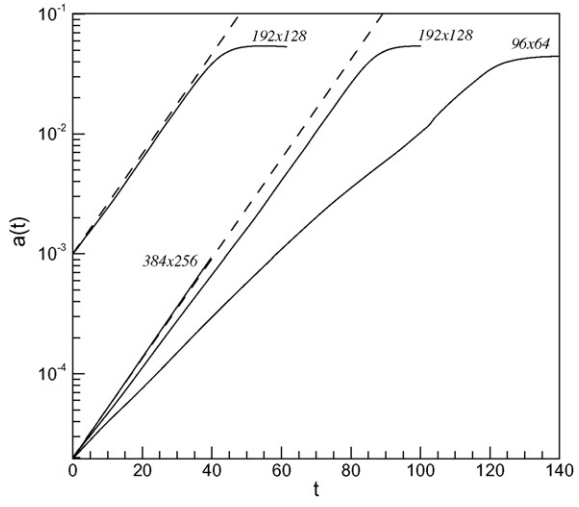

Fig. 4. Maximum perturbation height as a function of time for the same case as in Fig. 2, with $L = 1.5$. Solid and dashed lines represent the numerical simulation (for the grids indicated) and linear stability analysis, respectively. The numerically obtained amplitudes of the saturated waves are 0.054 and 0.044 for the 192×128 and 96×64 grids, respectively.

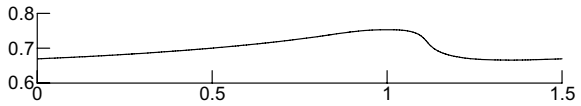

Fig. 5. Profile of saturated most dangerous mode ($L = 1.5$) for the same case as in Fig. 2 with a 192×128 grid (detail). Flow is from left to right.

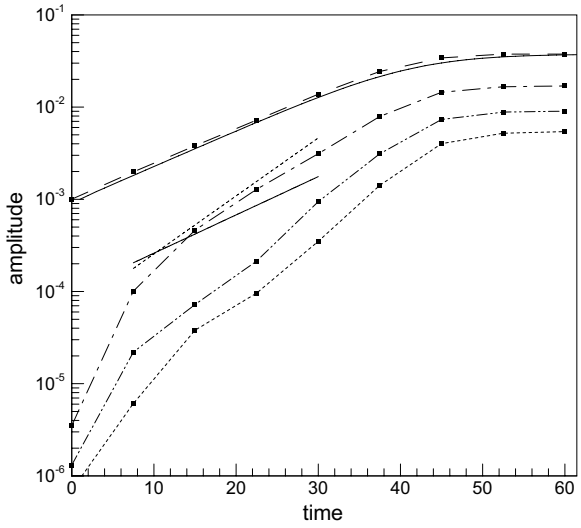

Fig. 6. Evolution of the Fourier spectrum for the most unstable mode ($L = 1.5$) with a 192×128 grid. Parameter values are the same as in Fig. 2. The solid curve is the solution of the Stuart–Landau theory with fitted coefficients. The dashed, dash-dotted, dash-dot-dotted and dotted lines represent the amplitude of the first, second, third and fourth harmonic, respectively, obtained from a Fourier transform. The solid line segment represents the growth rate of the fundamental mode corresponding to linear theory. The dotted segment represents that obtained when adding the growth rate of the first overtone.

comparison in Fig. 6. Evidently, the evolution of A_1 is well described by Eq. (10), and the Landau constant is positive – suggesting the existence of a supercritical bifurcation. But it would be necessary to conduct a complete parametric study in order to prove this (beyond the scope of this work), as even subcritical bifurcations can lead to amplitude saturation (King and McCready, 2000). Furthermore, although Eq. (10) is a convenient way to represent the results, there are concerns regarding its applicability (King and McCready, 2000). In particular, the case considered in Fig. 6 is for the linearly most unstable mode, which is rather far removed from the instability threshold (see Fig. 3a; the first overtone is linearly unstable).

The results in Fig. 6 also include the time evolution of the amplitude of three overtones. Although we have to be very cautious when drawing conclusions from these results, given the relatively small-amplitudes and the rather coarse discretisation, it is of interest to at least attempt to make sense of these data. In particular, it is a concern that the overtones in Fig. 6 grow faster than the fundamental mode, whereas the latter is linearly the most unstable. This could be due to non-linear effects (e.g., Barthelet et al., 1995; King and McCready, 2000), in particular, the results could show the significance of mode interactions. On the other hand, the present case is not sufficiently close to criticality for the arguments of weakly non-linear theory to be rigorously valid. There is an alternative explanation for the rapid growth of overtone amplitudes, which follows from the expectation that overtone amplitudes initially grow rapidly from zero (the initial condition) due to discretisation errors (i.e., the theoretical sinusoidal wave is slightly distorted). If, after an initial transient, the resulting shape of the wave remains approximately constant during an intermediate period in the simulations, the overtone amplitudes would be expected to grow at the same rate as the fundamental mode. A complication is that the first overtone is unstable according to linear theory. The first overtone could thus grow even faster than the fundamental mode. We have included in Fig. 6 line segments that represent the growth rate corresponding

to the sum of the growth rates of the fundamental mode and the first overtone from linear theory, and that of the fundamental mode itself. It is seen that the growth rate of the first overtone in the simulations is in between these two values. We note also that the growth rates of the amplitudes of the second and third overtone in the simulations are not far removed from these values, despite the fact that these are linearly stable. It could be argued that this is because they are associated with discretisation errors of the fundamental mode and the first overtone. (We have verified in additional simulations that shorter fundamental modes grow at a rate that compares with linear theory in a similar manner to the results given in Table 2 for $L = 1.5$.) We present and discuss further data on overtones for other cases later on in this section (Fig. 8) to further test the suggestions made above. If the initial growth is attributable to numerical error, the accuracy of growth rates of overtones at later times would naturally be a concern. However, the results presented here were found to be robust. For example, the time dependence of the amplitudes of the overtones was found to be almost identical when starting with the much smaller initial wave amplitude of 2×10^{-5} (e.g., at any value of the fundamental mode amplitude, the absolute amplitudes of the overtones are virtually the same in both cases). Also, we have seen in Fig. 4 that different values of the grid spacing only have a quantitative effect on the main result (the saturation of the linearly most unstable mode).

An approach to slug flow is observed for relatively long waves. We first investigate the evolution of a relatively long wave for the case corresponding to Fig. 2 (with $L = 8$). This wave is linearly unstable but has a relatively low linear growth rate (Fig. 3). The finest mesh that could be used without making the computational cost excessive was a 512×64 grid. It was found that the linear growth rate is underpredicted when using this grid, by about 14%. Hence the performance of the method happens to be better here than for the short waves at the same grid spacing (cf. Table 2). The height of the wave crest as a function of time is shown in Fig. 7. It is seen that the wave grows to at least double the amplitude attained by the linearly most unstable wave. The maximum wave amplitude is 0.1, and the wave is still growing (at least, in the case of the finest mesh, 512×64 grid, used here). We therefore investigate this wave growth in more detail here.

For relatively short times ($t < 60$), the growth rate is seen to be acceptably close to the value from linear theory (which is only slightly underpredicted, consistent with the findings in Table 2 for short waves). But, in contrast to the evolution of the short wave, there are sudden changes in the slope of the curves shown (this is seen for both values of the grid spacing used). Also, the growth rate increases significantly. The time evolution of the first four harmonics is shown in Fig. 8, together with the corresponding result for a simulation with a much larger initial amplitude. In Fig. 8b, the linear growth rate of the first overtone is larger than that of the fundamental mode. The amplitude of the first overtone is seen to eventually grow beyond that of the

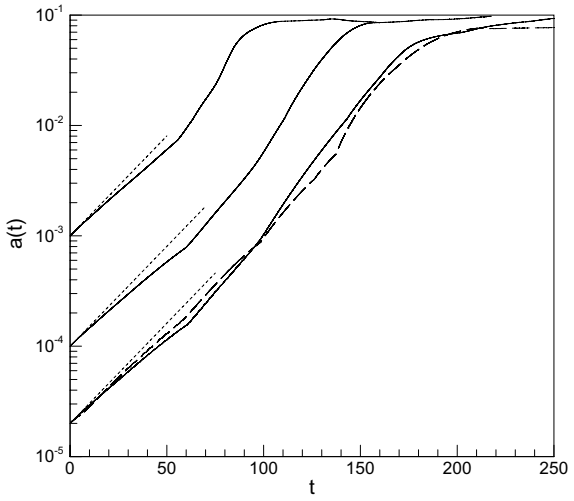

Fig. 7. Maximum perturbation height as a function of time from numerical simulations for the same case as in Fig. 2 with $L = 8$ for three different initial amplitudes 2×10^{-5}, 1×10^{-4} and 1×10^{-3}. Dashed and solid lines represent grids of 256×32 and 512×64, respectively. The short-dashed line represents linear stability theory.

fundamental mode, which would invalidate an assumption made in Stuart–Landau theory. The growth of the fundamental mode appears to be increased as a result. Subsequently, the first overtone seems to approach saturation, whereas the fundamental mode continues to grow, such that the fundamental mode then overtakes the first overtone again. Eventually, all overtones are suppressed whereas the fundamental mode continues to increase in amplitude. A qualitatively similar result is observed in Fig. 8a for an initially larger amplitude.

It may also be seen in Fig. 8a that the overtone amplitudes grow at rates in between the corresponding values obtained from linear theory for the overtone themselves (or somewhat less as may be expected from Fig. 4), and the values obtained when adding the growth rate of the fundamental mode, as suggested in the discussion of Fig. 6 above. It is encouraging to see that the results are much closer to the growth rates of the overtones themselves than in Fig. 6 (note that the solid line segments in that figure represent the growth rate of the fundamental mode from linear theory, not that of the overtones). This would be expected because

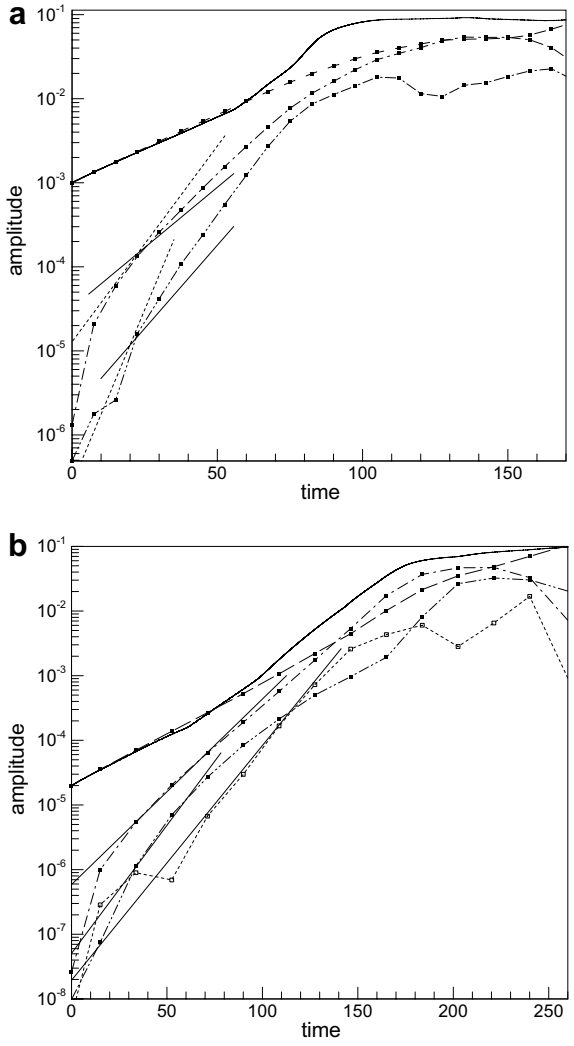

Fig. 8. Evolution of the Fourier spectrum for $L = 8$ using a 512×64 grid and an initial amplitude of 10^{-3} (a) and $2 \cdot 10^{-5}$ (b). The solid line is the amplitude based on the height of the wave crest. The dashed, dash-dotted and dash-dot-dotted lines with solid squares represent the amplitude of the first, second and third harmonic, respectively, obtained from a Fourier transform (the dotted line with open squares in (b) is the fourth harmonic). The parameter values are the same as in Fig. 7. The result for the fourth harmonic shows significant scatter (not shown) but does appear to be enslaved to the second harmonic. The solid line segments represent the growth rate corresponding to linear theory. The dotted segments represent that obtained when adding the growth rate of the fundamental mode.

the overtones are more unstable than the fundamental mode in the present case. We also note from comparing Fig. 8a and b that when the overtones are smaller compared to the fundamental mode, their growth rate is overpredicted to a larger degree. It is encouraging to see that, despite such differences between Fig. 8a and b regarding this comparison with the linear growth rates, the subsequent dynamics are qualitatively very similar. At late times, we see that the fundamental mode dominates at first, then the first overtone, and finally the fundamental mode again, and that the contributions of higher overtones become significant in the final stages of the simulation. We have verified that the results on a coarser (256×32) grid also lead to wave coalescence.

We show details of the change in wave shape in Figs. 9a–d and 10a–d. At time $t = 75$, the wave has been distorted somewhat, apparently due to amplification of shorter wavelength noise (Fig. 9a) as discussed above. These distortions evolve into disturbances of the initial profile, of wave length around 2. It is encouraging to see that this corresponds roughly to the most-dangerous mode (Fig. 3), corresponding to the rapid growth of the overtones observed in Fig. 8b. Thereafter, these short waves grow faster than the long wave that was imposed as the initial condition (Fig. 9b–d). The crests of the short waves are not identical, and, at later times, the short wave with the largest amplitude overtakes and merges with the other waves, thereby resulting in a single large wave structure, of wave length equal to the size of the domain (Fig. 10d). Hence the changes of slope seen in Fig. 7 occur when the highest point shifts between the competing peaks of shorter wavelength. The coalescence process was also observed when starting with a much larger initial amplitude, 10^{-3} instead of 2×10^{-5}.

A detailed comparison with experimental observations of slug initiation is of course difficult. Nevertheless, it is of interest to note the observations of Andritsos et al. (1989) that the first disturbances to appear on the interface are very small sinusoidal waves. They found that these suddenly give rise to a large-amplitude wave which leads to slug formation. Sometimes a few large-amplitude waves coalesce with one another before a slug is formed. Fan et al. (1993) showed that the initial small-amplitude, short-wavelength waves lead to a large-amplitude wave of longer wave length (roughly double the initial length) further downstream. The present work shows that such phenomena also can occur under laminar conditions.

The computational results also further elucidate the later stages of the wave development. In Fig. 10, instantaneous streamlines are shown. The streamlines were obtained by subtracting a wave speed from the instantaneous velocity field, then using a central-difference approximation for the vorticity, and solving the

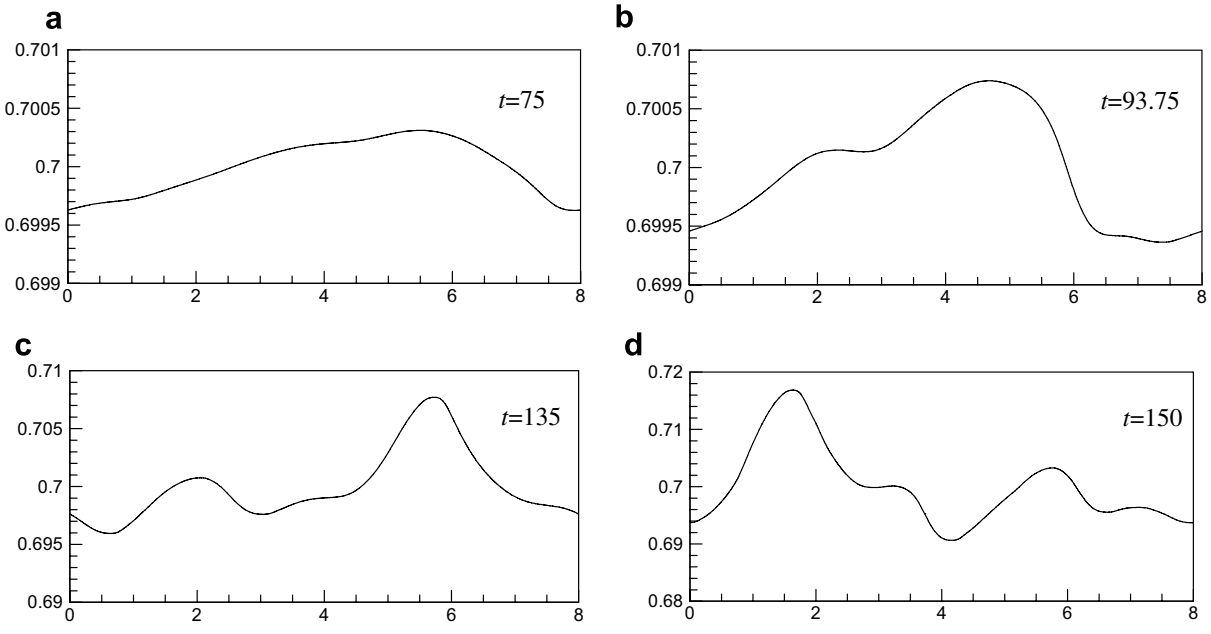

Fig. 9. Early stages of wave growth: spatial wave profiles for the same case as in Fig. 6; $L = 8$ and the grid is 512×64.

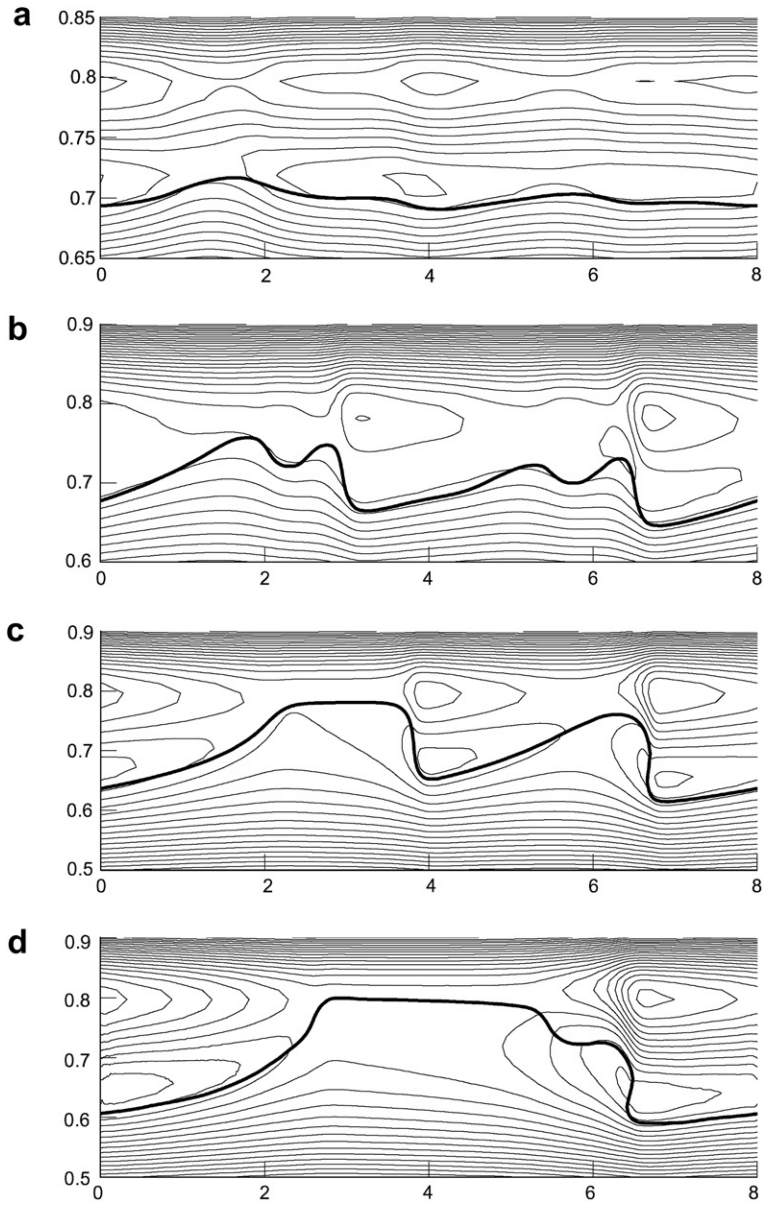

Fig. 10. Later stages of wave growth. Contour plots of the stream function in a frame of reference moving with the highest point of the wave. The thick line represents the interface. The parameters remain the same as in Fig. 7, at times $t = 150$ (a), 180 (b), 221.25 (c) and 262.5 (d).

Poisson-type equation for the stream function iteratively, also using a finite-difference method. The ''wave speed'' used here is the time derivative of the location of the highest point of the wave.

At intermediate times (Fig. 10a), the instantaneous streamlines are similar to the short wave Orr–Sommerfeld solution. Two layers of vortical structures are observed in the upper fluid, these are located above the wave troughs. At intermediate times (Fig. 10b), the counter-rotating vortices located above each trough grow, and together interact with the wave front in a complex manner, eventually leading to merging of short waves by ''filling-in'' the trough between two waves. A similar mechanism appears to lead to further merging at later times (Fig. 10c and d). Shortly after the time corresponding to Fig. 10d it appeared that spurious currents started to affect the interface shape. We return to late stages in the wave evolution further below.

In the results discussed above, discretisation errors lead to the formation of short waves. Key features of the subsequent growth appear to be the difference in amplitude of co-existing short waves, and the non-periodic distribution of these waves. Simulations starting with several short waves of equal amplitude, superimposed on a long wave, gave no indication of an approach to slug initiation.

Slug initiation can also be approached in other ways, such that the role of discretisation errors is further reduced. In Fig. 11, we show results from a simulation in which a wave of relatively large-amplitude (0.0125 times the channel height) was introduced (the wavelength was again 8; the other parameters are as in Fig. 2). Here, however, the corresponding velocity and pressure disturbances that would follow from linear theory for such a wave are not included (these perturbations would be too large, as explained at the end of the previous section). It is seen that, in this case, short waves do not have sufficient time to grow and merge; instead, slug initiation is approached by continuous deformation and growth of a long wave. Despite this difference with the results in Figs. 9 and 10, the instantaneous stream function in Fig. 11c is similar to that shown in Fig. 10d. Fig. 11d shows the reduced pressure, which is obtained by subtracting the hydrostatic contribution to the pressure and the linear axial pressure gradient.

At a late stage in the wave development, the tail of the wave is seen to steepen markedly (Figs. 10d and 11b). Fig. 12 shows the interpolated values of the normal and shear components of the viscous stress tensor and the pressure corresponding to Fig. 11c, and 13a shows the velocity profiles at the trough and crest of the wave. In Fig. 12a a retarding shear stress (which is directed to the left) is seen to be exerted by the upper fluid

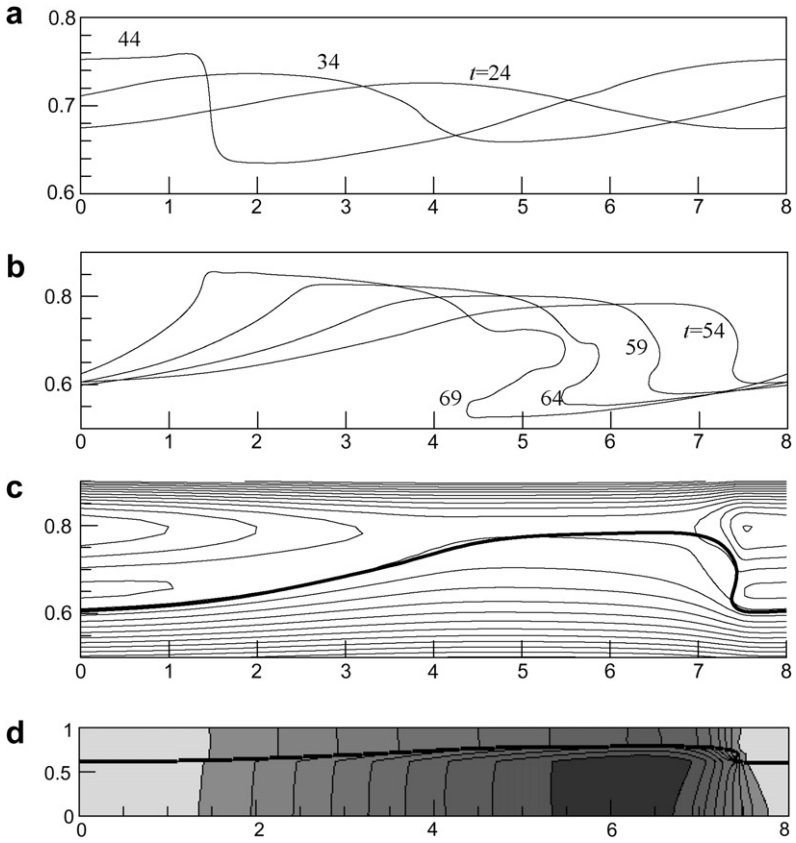

Fig. 11. Approach to slug initiation from continuous deformation of a single wave. Results are for the same case as in Fig. 7, but here a disturbance in the interface height of relatively large-amplitude (0.0125 of the channel height) is initially imposed, with no disturbance in the velocity or pressure. The grid size is 512×64. The interface shapes shown in (a) and (b) correspond to the times indicated. The instantaneous streamlines shown in (c) for $t = 54$ are in a frame of reference moving with the crest of the wave. The spacing in values of the stream function is 0.02. The corresponding contour plot of the reduced pressure is shown in (d), where the thick line represents the interface.

at the top of the wave, while the shear stress in the trough on the left-hand side of the figure is much larger (and is directed towards the right). Such an out-of-phase stress distribution is expected to lead to wave growth [see e.g., Hanratty, 1983 for similar arguments for linear instability mechanisms]. A complicating factor here is that the stress distribution is asymmetric with respect to the wave crest; the stress magnitude is higher in the troughs than at the crest. Overall, one would expect this to lead to distortion of the wave shape, in particular, to the steepening of the tail of the wave. We also note that, in Fig. 11d, the reduced pressure is seen to be in phase with the interface height (see also Fig. 11a), and will act to stabilise the wave. It is clear from Fig. 11d that the hydrostatic contribution still dominates the pressure disturbance in the lower fluid. For the benefit of one-dimensional model development, we have plotted the shear stress distribution at the walls for the same wave, in Fig. 12b. It is of interest that the shear stress does not vary very much along the walls.

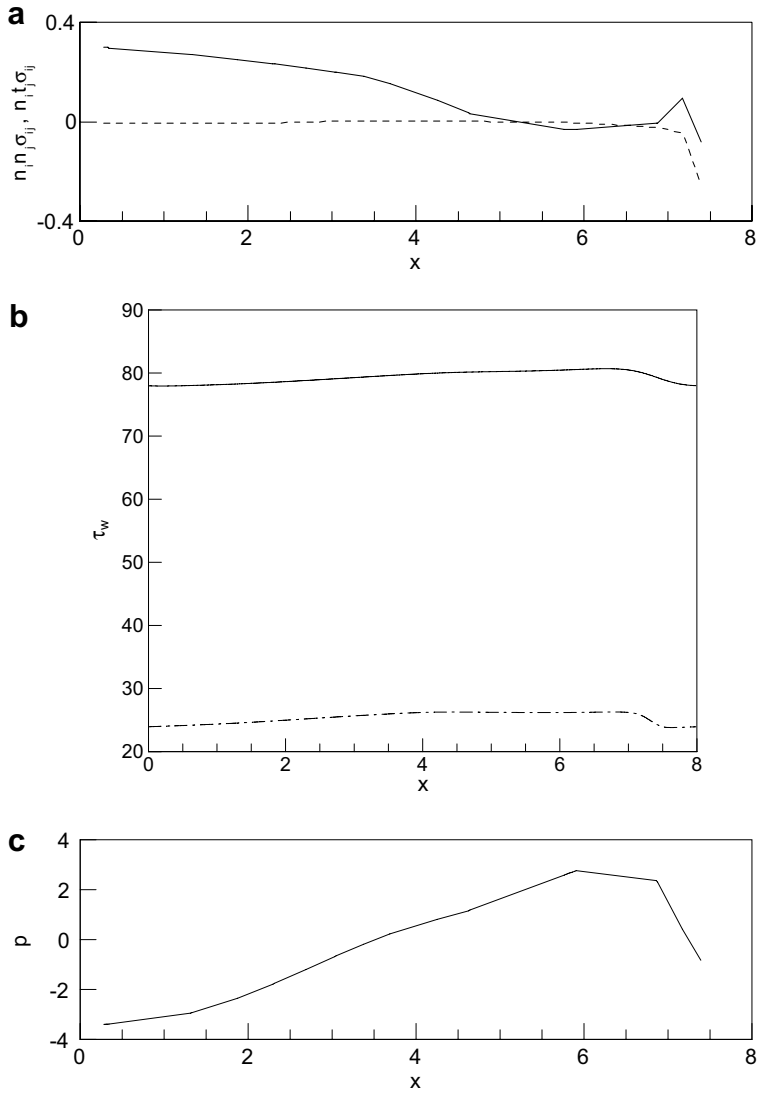

Fig. 12. Profiles of interfacial (a) and wall (b) stress components for the flow shown in Fig. 11c and d. In (a), the solid line shows the shear stress and the dashed line shows the normal stress. In (b), the solid and dashed lines show the magnitude of the shear stress at the bottom and top walls, respectively. (c) Reduced pressure. Note from Fig. 11c that the wave is turning over already at this time, explaining the rapid changes near $x = 7.4$. The data shown in (a) were obtained from the simulations by taking averaged values at cell vertices of the level-set function. Only grid cells were taken into account where this averaged value is less than 0.05 times the grid spacing and the vertex is located in the upper fluid.

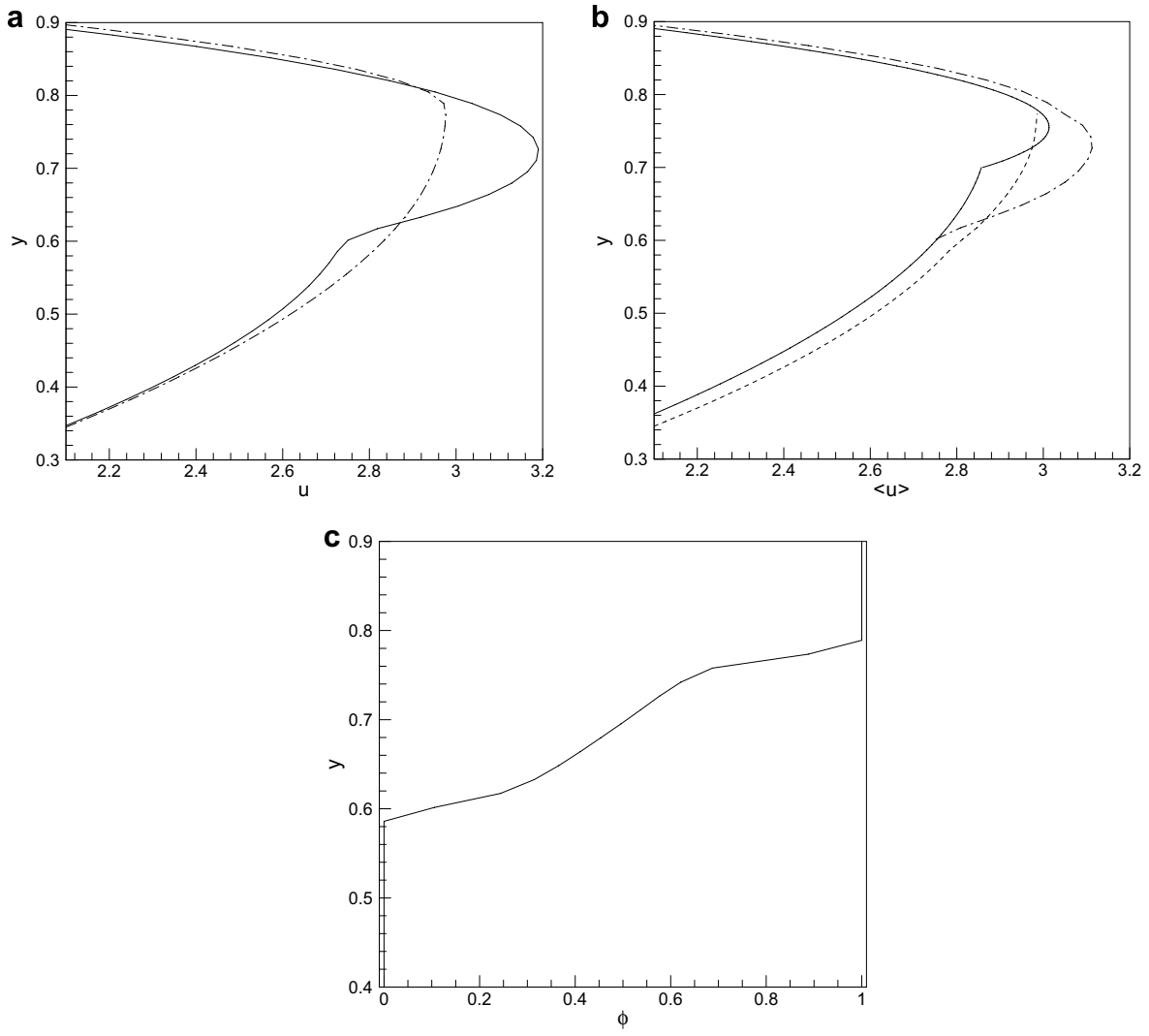

Fig. 13. Velocity profiles for the flow in Fig. 9c. (a) Velocity profile at the trough (solid line; $x = 0$) and crest (dash-dotted line; $x = 6$). (b) Velocity profile averaged over the wave length. Dashed line, fluid B; dash-dotted line, fluid A; solid line, initial (flat interface) velocity profile. (c) Profile of the averaged volume fraction of the upper fluid.

Finally, for possible modelling purposes of slug flows, line-averaged velocity profiles are shown in Fig. 13b, together with the initial velocity profile for a flat interface; the corresponding volume fraction of the upper fluid is shown in Fig. 13c. It is seen that the wave causes an increase in the maximum velocity. Also, the averaged profiles exhibit interphase slip at most points, even at the trough and crest of the wave. We also see from this figure that the wave speed (equal to 3.0) is larger than the averaged velocity in the lower fluid.

Although no full parametric study was performed, some additional simulations were performed to investigate whether the observations made here are more generally valid. Simulations for a value of Re five times larger (=2500), and an initial wave amplitude of 10^{-4} (all other parameters as before) showed virtually the same coalescence process observed in Fig. 10. The value of Ca was subsequently increased five-fold to 50; again, results qualitatively similar to those in Fig. 10 were observed (hence neither case is shown here). In simulations with a lower base-state interface height of $h = 0.68$, no approach to slug initiation was observed, although the growth rate for disturbances is significantly higher (see Fig. 3b). In such cases, depending on flow parameters, either a saturated travelling wave results, or atomisation events are approached.

5. Conclusions

We have presented results for the onset of the initiation of slug-type structures in 2D, two-phase stratified laminar pressure-driven channel flow. Numerical results were obtained using a level-set method for the simulation of 2D two-phase flows. Good agreement was obtained with (amongst other tests) an Orr–Sommerfeld-type stability analysis for the growth rate and wave speed of very small disturbances of the flow (to which the analysis is limited).

The numerical results show the non-linear evolution of the interface shape, once small disturbances have grown substantially. A tendency towards slug formation was observed when the initial interface level was sufficiently high. The linear theory and the subsequent energy analysis in Section 2 show that the most unstable mode is an interfacial mode of relatively short-wavelength, for the cases simulated here. The short waves saturate when the length of the periodic domain is set equal to the wave length, and longer waves are absent initially. The evolution of the amplitude of the fundamental mode could be well described by a Stuart–Landau equation in this case, with a positive Landau constant. We also found that at early times in this case, overtones can be enslaved by the fundamental mode due to numerical error if their linear growth rate is not sufficiently large, although the late-time dynamics seems to be affected only quantitatively.

In Section 3, short waves are observed to coalesce into large-amplitude longer waves when the length of the periodic domain is large. Evidently there is a need for a reduced theory that would represent such phenomena. The time evolution of the fundamental mode and overtones is more complex and it is argued that it would not be possible to model this using Stuart–Landau theory. Furthermore, it is shown that the growth and distortion of the large wave are associated with the shear stress being directed towards the trailing part of the wave crest. It is clear that the distribution of shear stress along the interface is very important for wave growth, so that simplified shear stress models that are commonly used in one-dimensional approaches are likely to lead to erroneous results. Further analysis would be needed to improve such simplified approaches to take into account the shear stress distribution in models of reduced dimensionality.

Results were also presented that are of potential use in further modelling efforts, including phase-averaged velocity profiles, and a volume fraction distribution. These could be used in future work on large-scale modelling of stratified flows, e.g., in approaches wherein the average flow is treated as consisting of two layers separated by a two-phase layer representing the wavy interface.

Although the results presented here show the important transition from the linear regime for infinitesimal waves to the onset of slug initiation, the numerical method used has posed some important restrictions on this study that must be removed in future work. The main restrictions are that the flows simulated are laminar, with relatively modest density and viscosity ratios. Despite the experimental observations summarised in Section 1, it remains unclear exactly how the corresponding transition to slug flow occurs in turbulent flow. Even linear theories published so far on this problem make the important assumption that the only significant role of turbulence is to change the averaged velocity profile. A further important restriction of the present work is that the flows simulated are two-dimensional. It is anticipated that 3D geometrical effects will be especially important during bridging events, i.e., the final stage of slug initiation. Finally, due to the excessive computational effort required, a full parametric study could not be conducted here; instead, a detailed investigation was conducted for a few representative values of the flow parameters.

Acknowledgements

This work has been undertaken within the Joint Project on Transient Multiphase Flows. The authors wish to acknowledge the contributions made to this project by the Engineering and Physical Sciences Research Council (EPSRC GR/S17765), Advantica, AspenTech, BP Exploration, Chevron, ConocoPhillips, ENI, ExxonMobil, FEESA, Granherne/ Subsea 7, Institutt for Energiteknikk, Institut Français du Pétrole, Norsk Hydro, Petrobras, Scandpower; Shell, SINTEF, Statoil and TOTAL.

Table A1
Convergence test for a slowly decaying travelling wave

N^2	E_N	$\log_2(E_N/E_{N/2})$
32^2	17.8	
64^2	7.05	1.34
128^2	3.14	1.17
256^2	1.42	1.14

Parameter values used are $n = 1$, $m = 1$, $\gamma = 1$, $Re_W = 100$, $k = 2\pi$, $h = 0.5$ and $(dx/a) = 0.3125$. Here E_N is the percentage deviation from the analytical solution.

Appendix A

It is instructive to check the numerical method against a well-established, explicit analytical solution for slowly decaying travelling waves, such that $\omega = \sqrt{\gamma(1 - e^{-2kH})/(k\rho)} - 2\nu k^2 \imath$ (Lamb, 1932). In this test, the fluids are density and viscosity-matched. The other parameter values used are $\gamma = 1$, $L = H = 1$ and $h = 0.5$. The wave amplitude is not vanishingly small compared with the grid spacing, so that keeping the wave amplitude constant whilst refining the mesh will result in convergence to a value that is not exactly the same as the theoretical prediction. Therefore, the amplitude of the initial wave was varied proportionally with the grid spacing (in this particular case, the ratio was 0.3125). In this way, refining the mesh will also amount to approaching the analytical limit more closely. Changing the amplitude, however, results in changing the Reynolds number associated with the wave motion, $Re_W = \varepsilon^2 kc/\nu$, which would result in an inconsistent comparison between results from different meshes. The viscosity is therefore chosen in this test such that Re_W is fixed at a value of 100. Results for the period of the wave for different values of the grid spacing, thus obtained, are shown in Table A1. Approximately first order convergence is obtained, consistent with other convergence tests (Spelt, 2005).

References

Andritsos, N., Hanratty, T.J., 1987. Influence of interfacial waves in stratified gas–liquid flows. Int. J. Multiphase Flow 33, 444–454.
Andritsos, N., Williams, L., Hanratty, T.J., 1989. Effect of liquid viscosity on the stratified-slug transition in horizontal pipe flow. Int. J. Multiphase Flow 15, 877–892.
Barthelet, P., Charru, F., Fabre, J., 1995. Experimental study of interfacial long waves in two-layer shear flow. J. Fluid Mech. 302, 23–53.
Belcher, S.E., Hunt, J.C.R., 1993. Turbulent shear flow over slowly moving waves. J. Fluid Mech. 251, 109–148.
Belcher, S.E., Hunt, J.C.R., 1998. Turbulent flow over hills and waves. Annu. Rev. Fluid Mech. 30, 507–538.
Benjamin, T.B., 1959. Shearing flow over a wavy surface. J. Fluid Mech. 6, 161.
Boeck, T., Zaleski, S., 2005. Viscous versus inviscid instability of two-phase mixing layers with continuous velocity profile. Phys. Fluid 17, 032106.
Boeck, T., Li, J., López-Pagés, E., Yecko, P., Zaleski, S., 2006. Ligament formation in sheared liquid–gas layers. Theor. Comput. Fluid Dyn. 21, 59–76.
Boomkamp, P.A.M., Miesen, R.H.M., 1996. Classification of instabilities in parallel two-phase flow. Int. J. Multiphase Flow 22 (Suppl.), 67–88.
Boomkamp, P.A.M., 1998. Stability of parallel two-phase flow. PhD Thesis, University of Twente.
Coward, A.V., Renardy, Y.Y., Renardy, M., Richards, J.R., 1997. Temporal evolution of periodic disturbances in two-layer Couette flow. J. Comput. Phys. 132, 346–361.
Davies, S.R., 1992. Studies of two-phase intermittent flow in pipelines. PhD Thesis, University of London.
Davis, R.E., 1969. On the high Reynolds number flow over a wavy boundary. J. Fluid Mech. 36, 337.
Fan, Z., Lusseyran, F., Hanratty, T.J., 1993. Initiation of slugs in horizontal gas–liquid flows. AIChE J. 39, 1741–1753.
Fukano, T., Inatomi, T., 2003. Analysis of liquid film formation in a horizontal annular flow by DNS. Int. J. Multiphase Flow 29, 1413–1430.
Hale, C.P., 2000. Slug formation, growth and decay in gas–liquid flows. PhD Thesis, University of London.
Hanratty, T.J., 1983. Interfacial instabilities caused by air flow over a thin liquid layer. In: Waves on Fluid Interfaces. Academic, New York, pp. 221–259.
Hewitt, G.F., 1982. Flow regimes. In: Hetsroni, G. (Ed.), Handbook of Multiphase Systems, Hemisphere (Chapter 2).
Hinch, E.J., 1984. A note on the mechanism of the instability at the interface between two shearing fluids. J. Fluid Mech. 144, 463–465.
Hirsch, C., 1988. Numerical computation of internal and external flows. In: Fundamentals of Numerical Discretization, vol. 1. Wiley.
Hooper, A.P., Boyd, W.G.C., 1983. Shear-flow instability at the interface between two viscous fluids. J. Fluid Mech. 128, 507–528.

Hu, H.H., Joseph, D.D., 1989. Lubricated pipelining: stability of core-annular flow. Part 2. J. Fluid Mech. 205, 359–396.
Kang, M., Fedkiw, R.P., Liu, X.-D., 2000. A boundary condition capturing method for multiphase incompressible flow. J. Sci. Comput. 15, 323–360.
Kelly, R.E., Goussis, D.A., Lin, S.P., Hsu, F.K., 1989. The mechanism for surface wave instability in film flow down an inclined plane. Phys. Fluid A1, 819–828.
King, M.R., McCready, M.J., 2000. Weakly nonlinear simulation of planar stratified flows. Phys. Fluid 12, 92–102.
Kordyban, E., 1985. Some details of developing slugs in horizontal 2-phase flow. AIChE J. 31, 802–806.
Kuru, W.C., Sangalli, M., Uphold, D.D., McCready, M.J., 1995. Linear stability of stratified channel flow. Int. J. Multiphase Flow 21, 733–753.
Lafaurie, B., Nardone, C., Scardovelli, R., Zaleski, S., Zanetti, G., 1994. Modelling merging and fragmentation in multiphase flows with SURFER. J. Comput. Phys. 113, 134–147.
Lamb, H., 1932. Hydrodynamics, sixth ed. Cambridge University Press.
Li, J., Renardy, Y., 1999. Direct simulation of unsteady axisymmetric core-annular flow with high viscosity ratio. J. Fluid Mech. 391, 123–149.
Lin, P.Y., Hanratty, T.J., 1986. Prediction of the initiation of slugs with linear stability theory. Int. J. Multiphase Flow 12, 79–98.
Magnaudet, J., Bonometti, T., Benkenida, A., 2006. The modelling of viscous stresses for computing incompressible two-phase flows on fixed grids. Preprint.
Manolis, I.G., 1995. High pressure gas–liquid slug flow. PhD Thesis, Imperial College London.
Mata, C., Pereyra, E., Trallero, J.L., Joseph, D.D., 2002. Stability of stratified gas–liquid flow. Int. J. Multiphase Flow 28, 1249–1268.
Miesen, R.H.M., Boersma, B.J., 1995. Hydrodynamic stability of a sheared liquid film. J. Fluid Mech. 301, 175–202.
Miles, J.W., 1967. On the generation of surface waves by shear flows. Part 5. J. Fluid Mech. 30, 163.
Morland, L.C., Saffman, P.G., 1993. Effect of wind profile on the stability of wind blowing over water. J. Fluid Mech. 252, 383–398.
van Noorden, T.L., Boomkamp, P.A.M., Knaap, M.C., Verheggen, T.M.M., 1998. Transient growth in parallel two-phase flow: analogies and differences with single-phase flow. Phys. Fluid 10, 2099.
Smith, M.K., 1990. The mechanism for the long-wave instability in thin liquid films. J. Fluid Mech. 217, 469–485.
South, M.J., Hooper, A.P., 1999. Linear growth in two-fluid plane Poiseuille flow. J. Fluid Mech. 381, 121–139.
Spelt, P.D.M., 2005. A level-set approach for simulations of flows with multiple moving contact lines with hysteresis. J. Comput. Phys. 207, 389.
Spelt, P.D.M., 2006. Shear flow past two-dimensional droplets pinned or moving on an adhering channel wall at moderate Reynolds numbers: a numerical study. J. Fluid Mech. 561, 439–463.
Sussman, M., Almgren, A.S., Bell, J.B., Colella, P., Howell, L.H., Welcome, M.L., 1999. An adaptive level set approach for incompressible two-phase flows. J. Comput. Phys. 148, 81–124.
Taitel, Y., Dukler, A.E., 1976. A model for predicting flow regime transitions in horizontal and near horizontal gas–liquid flow. AIChE J. 22, 47–55.
Tauber, W., Unverdi, S.O., Tryggvason, G., 2002. The nonlinear behaviour of a sheared immiscible fluid interface. Phys. Fluid 14, 2871–2885.
Thorsness, C.B., Morrisone, P.E., Hanratty, T.J., 1978. A comparison of linear theory with measurements of the shear stress along a solid wave. Chem. Eng. Sci. 33, 579.
Ujang, P.M., Lawrence, C.J., Hale, C.P., Hewitt, G.F., 2006. Slug initiation and evolution in two-phase horizontal flow. Int. J. Multiphase Flow 32, 527–552.
Yiantsios, S.G., Higgins, B.G., 1988. Linear stability of plane Poiseuille flow of two superposed fluids. Phys. Fluid 31, 3225–3238, and correction: A1, 897.
Yecko, P., Zaleski, S., 2005. Transient growth in two-phase mixing layers. J. Fluid Mech. 528, 43–52.
Yecko, P., Zaleski, S., Fullana, J.-M., 2002. Viscous modes in two-phase mixing layers. Phys. Fluid 14, 4115.
Yih, C.-S., 1967. Instability due to viscosity stratification. J. Fluid Mech. 27, 337–352.